



Kashf Journal of Multidisciplinary Research

Vol: 02 - Issue 09 (2025)

P-ISSN: 3007-1992 E-ISSN: 3007-200X

https://kjmr.com.pk

HIGH-EFFICIENCY LEAD-FREE PEROVSKITE SOLAR CELLS: INSIGHTS FROM PARAMETER OPTIMIZATION IN RbGeI₃ DEVICES VIA DEVICE SIMULATION

Azhar Nawaz

Faculty of Sciences, Department of Physics, The Superior University Lahore, Pakistan

Muhammad Yasir Nawaz Khan

Faculty of Sciences, Department of Physics, The Superior University Lahore, Pakistan

Ayaz Husnain

Faculty of Sciences, Department of Physics, University of Agriculture Faisalabad, Pakistan

Article Info





This article is an open access article distributed under the terms and conditions of the Creative Commons Attribution (CC BY) license https://creativecommon

s.org/licenses/by/4.0

Abstract

Perovskite solar cells (PSCs) have attracted considerable interest in recent years owing to their remarkable power conversion efficiencies and promising prospects for cost-effective fabrication. This study reports the numerical optimization of a thin-film perovskite solar cell architecture consisting of FTO/IGZO/RbGeI₃/CuSbS₂/Au, where IGZO functions as the electron transport layer, RbGeI₃ serves as the light-harvesting perovskite absorber, and CuSbS₂ is employed as the hole transport layer. A systematic variation of the absorber, ETL, and HTL layer thicknesses, along with their respective electron affinities, was conducted to evaluate the impact on key photovoltaic parameters, including the V_{OC}J_{SC}, FF, and PCE. The optimized absorber thicknesses markedly enhance J_{SC} and PCE, achieving a maximum efficiency of approximately 29.3% with a 700 nm RbGeI3 layer. The electron affinity of IGZO was found to play a critical role in facilitating efficient charge extraction, with the highest PCE obtained at 4.28 eV. Likewise, modulation of the CuSbS₂ HTL thickness yielded progressive improvements in PCE, reaching up to 29.37%. The concurrent optimization of thickness parameters and interfacial band alignment led to substantial increases in FF and overall device efficiency. This establishes a useful reference point for advancing future research in this field.

Keywords:

Lead-Free perovskite Solar cell, Numerical Simulation, SCAPS 1-D, RbGeI₃, Optoelectrical Performance, IGZO ETL, CuSbS₂ HTL

1. INTRODUCTION

The escalating global energy demand, driven by urbanization and technological advancement, remains predominantly dependent on fossil fuels, leading to severe environmental degradation and climate change. A transition toward renewable resources such as wind, hydro, and solar power is therefore essential. Among these, solar energy is particularly auspicious due to its abundance, which has stimulated extensive research in photovoltaics. By enabling direct conversion of photons into electricity, photovoltaic technology provides a practical pathway to decarbonization. In particular, perovskite solar cells have emerged as a transformative innovation, demonstrating rapid improvements in efficiency and offering cost-effective, scalable fabrication, thereby positioning them as a leading candidate for sustainable energy solutions [1-6]. Perovskites, semiconducting materials with a tunable ABX₃ structure, have proven to be highly effective for solar cells. In this structure, A is a monovalent organic (e.g., MA⁺, FA⁺) or inorganic (Cs⁺) cation, B is a divalent metal cation (Pb²⁺, Sn²⁺), and X is a halide anion (I⁻, Br⁻). This composition yields exceptional optoelectronic properties ideal for photovoltaics [7-10]. Methylammonium lead halide perovskites (MAPbI₃) are widely used in PSCs due to their low-cost synthesis and facile processing. However, lead toxicity poses serious environmental and health risks, hindering large-scale commercialization. Despite this, PSCs have achieved remarkable PCEs, rivaling silicon photovoltaics. Addressing instability and toxicity remains crucial, driving research into lead-free, perovskite-inspired alternatives with comparable optoelectronic properties [11]. Tin (Sn²⁺)-based materials are regarded as promising lead-free absorbers but are limited by inherent instability. Their facile oxidation to Sn⁴⁺ under ambient conditions induces selfdoping, creating excess holes that intensify non-radiative recombination. This deterioration in semiconductor quality ultimately lowers photovoltaic efficiency and shortens device lifetime [12, 13]. Incorporating rubidium cations (Rb⁺) into the perovskite lattice enhances crystal symmetry and expands the lattice constant, thereby reducing defect density and improving charge transport. Among lead- and tinfree absorbers, RbGeI₃ has emerged as a promising candidate, offering structural stability and the potential for high photovoltaic efficiency, making it attractive for future commercialization of perovskite solar cells [14]. The perovskite derivative RbGeI₃ presents significant advantages for photovoltaics, foremost being its environmentally benign, non-toxic composition. It possesses a highly favorable direct bandgap of ~1.31 eV and a superior absorption coefficient, enabling efficient photon harvesting. These pivotal optoelectronic properties underpin its prominence in solar cell research. Furthermore, RbGeI₃ exhibits enhanced stability and reduced chemical reactivity, addressing critical durability challenges in the commercialization of perovskite devices [15]. A comprehensive SCAPS-1D simulation of an FTO/TiO₂/RbGeI₃/MoO₃/C architecture, utilizing a cost-effective carbon electrode, demonstrates the exceptional potential of the nontoxic RbGeI₃ absorber. The optimized device achieved a remarkable power conversion efficiency of 29.47% [16]. A numerical simulation was conducted to evaluate a lead-free inorganic perovskite photovoltaic architecture, employing an RbGeI₃ absorber layer coupled with a solution-processed CuCrO₂ delafossite HTL. The optimized device demonstrated a PCE of 23.8%, with a V_{OC} of 0.89 V, a J_{SC} of 33.7 mA cm⁻², and an FF of 79.2%. Performance analysis identified Shockley-Read-Hall recombination at the perovskite/HTL heterointerface as the principal loss mechanism. At the same time, temperature-dependent simulations confirmed excellent thermal operational stability, affirming the viability of this inorganic configuration for enhanced durability [17]. HTL-free RbGeI₃/KSnI₃ heterojunction solar cell demonstrates significantly enhanced performance over single-absorber devices. Optimized energy level alignment

strengthens the built-in electric field, facilitating superior carrier extraction and yielding a remarkable power conversion efficiency[18]. Researchers investigated a hole-transport-layer-free photovoltaic architecture via numerical simulation with SCAPS-1D. Strategic optimization of the electron transport and light-absorbing layer thicknesses to 0.08 µm and 0.40 µm, respectively, culminated in a stabilized power conversion efficiency of 3.60%. These findings underscore the structure's intrinsic potential for efficient photon harvesting and charge carrier generation [19]. By optimizing a wide-bandgap 1.31 eV RbGeI₃ perovskite solar cell, absorber thickness (0.6 µm) was identified as a critical performance factor. The optimized device achieved a notable efficiency of 24.62%, with a V_{OC} of 0.99 V, J_{SC} of 33.20 mA/cm², and FF of 82.8%, while exhibiting favorable series 2 Ω · cm² and shunt 10³ Ω · cm² resistances [20]. Utilizing pristine TiO₂ and TiO₂/graphene nanocomposites as ETLs at assorted concentrations, in conjunction with a NiO HTL, achieved significant performance enhancements. The integration of the nanocomposite ETL markedly improved photovoltaic metrics compared to the baseline pristine TiO₂, which delivered an initial efficiency of 24.91% [21]. Critical device parameters, including layer thickness, doping concentrations, defect densities, and series/shunt resistances, were systematically optimized. To enhance economic viability, carbon is proposed as a stable, cost-effective alternative to conventional gold back contact, with the optimized structure exhibiting superior quantum efficiency throughout the visible spectrum and robust thermal stability [22]. The Electron Transport Layer extracts electrons from the perovskite absorber and blocks holes, while the Hole Transport Layer facilitates hole extraction and blocks electrons. This selective carrier management minimizes recombination losses at the contacts, thereby enhancing the open-circuit voltage and overall device performance [23]. An efficient hole-transport material must possess a matched band alignment, high hole mobility, and optimal optoelectronic properties, alongside cost-effectiveness and simple processing. While organic HTMs like PEDOT:PSS and PTAA have enabled high-performance perovskite solar cells, they are often plagued by low conductivity, hygroscopicity, high cost, and complex synthesis, hindering their commercial viability [24]. CdS is a potential ETL; its utilization is problematic. Primarily, the material contains toxic cadmium, posing environmental risks. Furthermore, its narrow band gap (~2.45 eV) results in parasitic absorption of high-energy photons in the blue-green spectrum. This competitively reduces light availability for the perovskite layer, ultimately degrading device performance [25].

In this research, the FTO/IGZO/RbGeI₃/CuSbS₂/Au structure is used for simulation, in which Indium Gallium Zinc Oxide (IGZO) is commonly employed as an ETL in perovskite solar cell simulations because of its superior electron mobility, wide bandgap, and outstanding optical transparency. Its advantageous band alignment with perovskite materials facilitates effective electron extraction, minimizes recombination losses, and enhances device stability, outperforming conventional ETL materials [26]. Copper Antimony Sulfide (CuSbS₂) is utilized as HTL in perovskite solar cells due to its optimal valence band alignment, excellent hole mobility, and broad bandgap. It facilitates efficient hole extraction while effectively blocking electrons and enhancing thermal and chemical durability. Some parameters, like thickness and electron affinity of the harvesting layer, ETL, and HTL, are optimized to obtain maximum cell efficiency [27].

2. Methodology

A range of simulation platforms, such as SCAPS, AMPS, and COMSOL, are commonly employed for computational analysis of solar cell performance. In the present work, the Solar Cell Capacitance Simulator (SCAPS), a program developed in the C programming language at the University of Ghent, was utilized to carry out the simulations[28]. In this work, the FTO/IGZO/RbGeI₃/CuSbS₂ structure is used for simulation with an AM1.5G spectrum light intensity (1000 W/m²), The bandgap energy is symbolized by E_g, while the electron affinity is indicated by χ , and the dielectric permittivity by ϵ_r . The effective density of states in the conduction and valence bands is denoted as NC and NV, respectively. In addition, the defect concentration N_t, acceptor doping level N_A, donor doping level N_D, and the charge carrier mobilities of electrons μ_n and holes μ_p are defined. The thermal velocities of both electrons and holes are considered to be 10⁷ cm/s, as shown in Table 1. By using the SCAPS-1D for simulations of RbGeI₃ V_{OC}, J_{SC}, FF, and PCE are obtained as 1.0055 V, 33.1656 mA cm⁻², 86.8736, and 29.32% respectively.

Perimeter	RbGeI3	IGZO	CuSbS ₂
Thickness nm	400	100	100
Band gap Eg eV	1.31	3.05	1.5
Electron affinity χ eV	3.9	4.16	3.9
Dielectric permittivity ε _r	23.01	10	14.6
CB effective density of state N _C 1/cm ³	2.80E+19	5.00E+18	2.20E+18
VB effective density of state Nv 1/cm ³	1.40E+19	5.00E+18	1.80E+19
Electron thermal velocity cm/s	1.00E+07	1.00E+07	1.80E+07
Hole thermal velocity cm/s	1.00E+07	1.00E+07	1.00E+07
Electron mobility cm ² /Vs	2.86E+01	1.50E+01	6.00E+01
Hole mobility cm ² /Vs	2.73E+01	1.00E-01	2.00E+01
Shallow uniform donor density N _D 1/cm ³	0.00E+00	1.00E+18	0.00E+00
Shallow uniform acceptor density N _A 1/cm ³	1.00E+18	0.00E+00	1.00E+20
Defect density N _t 1/cm ³	1.00E+14	1.00E+14	1.00E+14

Table 1. Initial Cell Perimeter for Simulation

Perimeter	RbGeI ₃	IGZO	CuSbS ₂
Thickness nm	700	100	100
Band gap eV	1.31	1.5	3.05
Electron affinity eV	3.85	4.28	3.9
Dielectric permittivity	23.01	14.6	10
CB effective density of state 1/cm ₃	2.80E+19	2.20E+18	5.00E+18
VB effective density of state 1/cm ₃	1.40E+19	1.80E+19	5.00E+18
Electron thermal velocity cm/s	1.00E+07	1.80E+07	1.00E+07
Hole thermal velocity cm/s	1.00E+07	1.00E+07	1.00E+07
Electron mobility cm ² /Vs	2.86E+01	6.00E+01	1.50E+01
Hole mobility cm ² /Vs	2.73E+01	2.00E+01	1.00E-01
Shallow uniform donor density N _D 1/cm ³	0.00E+00	0.00E+00	1.00E+18

Shallow uniform acceptor density N _A 1/cm ³	1.00E+18	1.00E+20	0.00E+00
Defect density N _t 1/cm ³	1.00E+14	1.00E+14	1.00E+14

Table 2. Optimized Cell Perimeters

3. Results and Discussion

3.1 Influence of the thickness of the absorber on cell performance

The simulation results elucidate the thickness-dependent characteristics of RbGeI₃ absorber layers in perovskite solar cells. As the absorber thickness increases from 300 nm to 700 nm, a gradual diminution in the V_{OC} is observed from 1.0245 V to 1.0055 V. This decrease is primarily attributed to intensified bulk recombination within the thicker films [29], which marginally impairs the voltage. Conversely, the J_{SC} demonstrates a consistent increase from 29.04 mA/cm² to 33.16 mAcm⁻², resulting from enhanced photon absorption and increased charge carrier generation with increasing material thickness [30]. The FF remains essentially invariant (~87%), indicating stable charge transport mechanisms and negligible resistive losses despite variations in thickness. Consequently, the power conversion efficiency exhibits a notable enhancement, rising from 25.93% at 300 nm to 29.32% at 700 nm, as shown in table with the improvement predominantly driven by the elevated J_{SC} .

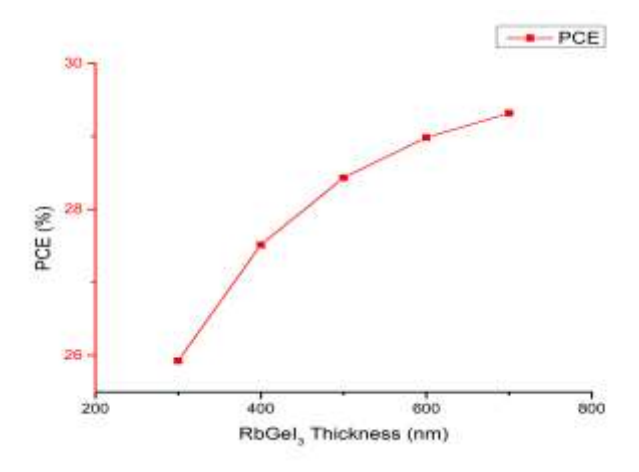


Figure 1. Effect of the Thickness of the Absorber Layer on PCE

RbGeI3 Thickness (nm)	VOC (V)	JSC	FF	PCE
300	1.0245	29.0417	87.1415	25.9265
400 500	1.0183 1.0134	31.0377 32.258	87.0545 86.9771	27.5138 28.4331
600	1.0092	33.04	86.9178	28.983
700	1.0055	33.1656	86.8736	29.3164

Table 3.RbGeI₃ Thickness effect on Cell Output

3.2 Influence of the Thickness of ETL

Increasing the IGZO thickness from 50 nm to 250 nm induces a slight decline in $V_{\rm OC}$ from 1.0056 V to 1.0052 V, mainly due to elevated series resistance and minor recombination at the ETL interface. The $J_{\rm SC}$ similarly decreases gradually, from 33.66 mA/cm² to 33.31 mA/cm², because of diminished optical transmittance at higher thicknesses, limiting photon absorption. The fill factor FF shows a marginal improvement from 86.86% to 86.91%, reflecting subtle enhancements in charge extraction uniformity and decreased shunting. Consequently, the PCE declines from 29.40% to 29.10%, implying that thinner IGZO layers around 50 to 100 nm optimize the trade-off between optical transparency and electron transport [31], thereby maximizing device performance.

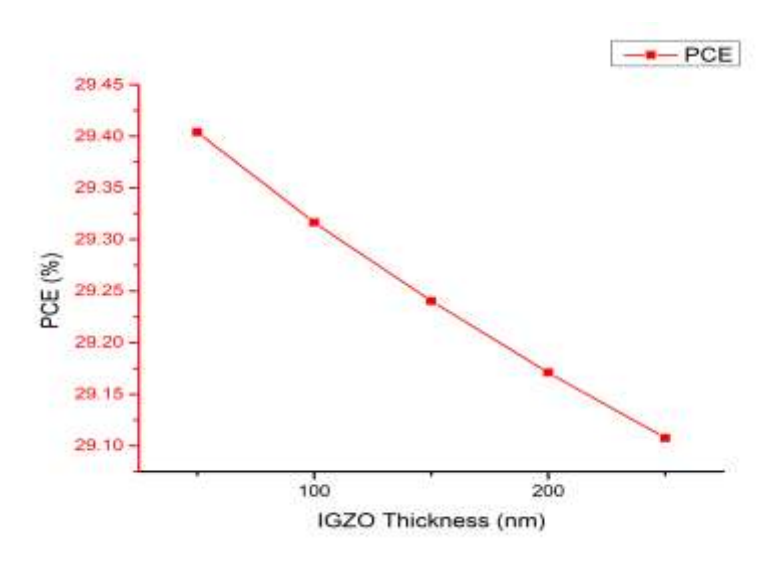


Figure 2.Effect of IGZO on Cell PCE

IGZO Thickness (nm)	VOC (V)	JSC	FF	PCE
50	1.0056	33.6602	86.8596	29.404
100	1.0055	33.5616	86.8736	29.3164
150	1.0054	33.473	86.8868	29.2403
200	1.0053	33.3927	86.8976	29.171
250	1.0052	33.3192	86.9076	29.1076

Table 4.Effect of IGZO on Cell PCE

3.3 Influence of the Thickness of HTL

The results illustrate the impact of CuSbS₂ layer thickness on the photovoltaic performance of RbGeI₃-based perovskite solar cells. As the CuSbS₂ thickness increases from 100 nm to 250 nm, the V_{OC} remains essentially unchanged at approximately 1.0055 V, indicating a negligible effect of thickness on voltage generation since recombination dynamics remain largely unaffected. Conversely, J_{SC} shows a slight but steady increase from 33.56 mA/cm² to 33.62 mA/cm², attributable to enhanced photon absorption and

improved charge extraction with thicker CuSbS₂ layers [32]. The FF remains almost constant (~86.87%), reflecting robust charge transport and minimal resistive or recombination losses over the examined thickness range. Consequently, the PCE exhibits a modest but consistent enhancement, rising from 29.32% at 100 nm to 29.37% at 250 nm. These findings imply that moderate increments in HTL thickness improve J_{SC} and PCE without undermining device reliability.

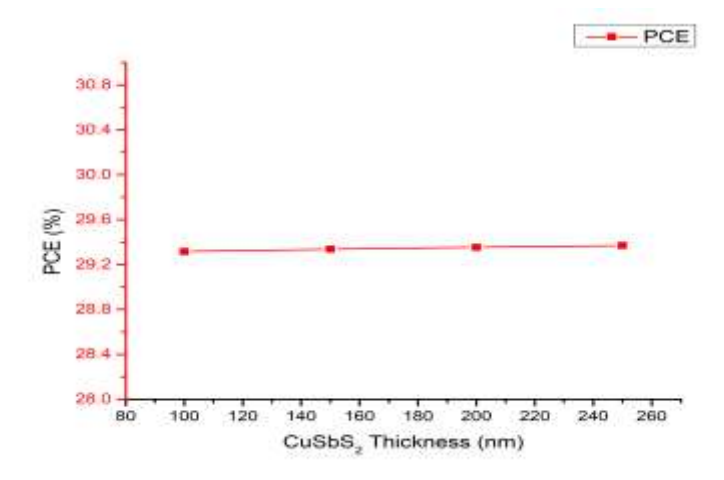


Figure 3. Effect of CuSbS2 on PCE

CuSBS ₂ Thickness (nm)	VOC (V)	JSC	FF	PCE
100	1.0055	33.5616	86.8737	29.3164
150	1.0055	33.5833	86.8737	29.3363
200	1.0055	33.6026	86.8735	29.3537
250	1.0056	33.6199	86.8726	29.369

Table 5.Effect of CuSbS2 on PCE

3.4 Effect of Electron Affinity on Harvesting Layer

The variation of RbGeI₃ bandgap energy from 3.85 eV to 4.05 eV affects device performance primarily through modulation of the absorber electron affinity (χ), which dictates interfacial band alignment with the adjacent transport layers. As the bandgap increases, the slight reduction in electron affinity elevates the conduction band edge relative to the ETL, thereby altering the conduction band offset (CBO) [33]. This less favorable alignment facilitates interfacial recombination, explaining the gradual decline in V_{OC} from 1.0184 V to 1.0174 V and the minor decrease in FF from 87.05% to 86.97%. The J_{SC} remains nearly unchanged (~31.03 mA/cm²), as photon absorption and carrier generation are not significantly influenced within this narrow bandgap window. Consequently, the PCE decreases slightly from 27.51% to 27.46%. These findings highlight that precise control of absorber electron affinity is essential to preserve favorable band alignment, suppress recombination losses, and sustain optimal photovoltaic performance.

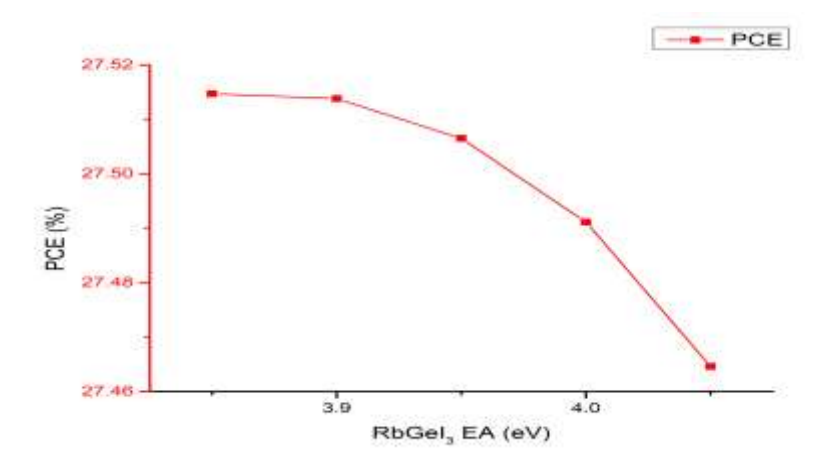


Figure 4. Effect of RbGeI₃ EA on PCE

RbGeI3 EA (eV)	VOC (V)	JSC	FF	PCE
3.85	1.0184	31.037	87.0502	27.5147
3.9	1.0183	31.037	87.0545	27.5138
3.95	1.0181	31.0383	87.0448	27.5065
4	1.0178	31.0386	87.0194	27.4911
4.05	1.0174	31.0184	86.972	27.4646

Table 6.Effect of RbGeI₃ EA on PCE

3.5 Effect of Electron Affinity of ETL on Cell Performance

The simulation findings can be elucidated by analyzing the role of the ETL's electron affinity (χ) in governing interfacial band alignment with the absorber. As the IGZO bandgap increases from 4.12 eV to 4.28 eV, the corresponding adjustment in electron affinity alters the CBO at the IGZO/RbGeI3 interface. At lower band gaps, 4.12 eV, the unfavorable CBO facilitates interfacial recombination [34], thereby diminishing both the FF and the PCE. With progressive bandgap enlargement from 4.20eV to 4.24 eV, the refined electron affinity establishes a more compatible alignment with the conduction band of RbGeI3, effectively suppressing recombination pathways and enhancing electron extraction. This accounts for the continuous rise in FF from 85.0% to 88.1% and the modest increase in V_{OC} . At 4.28 eV, the optimized electron affinity provides the most favorable interfacial configuration, yielding an elevated V_{OC} of 1.038 V and a maximum PCE of 27.84%.

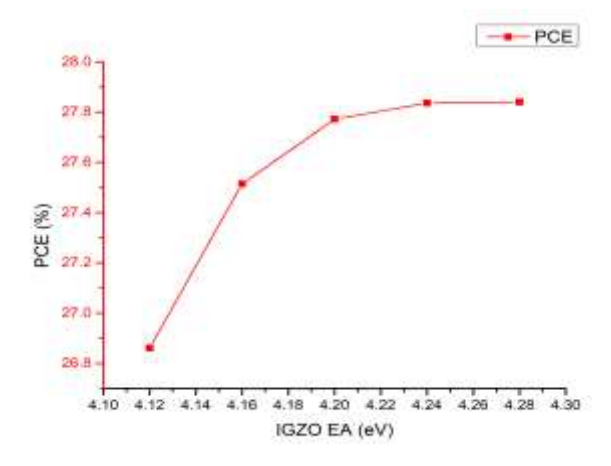


Figure 5. Effect of IGZO EA on PCE

IGZO EA (eV)	VOC (V)	JSC	FF	PCE
4.12	1.018	31.0366	85.0154	26.861
4.16	1.0184	31.037	87.0502	27.5147
4.2	1.0184	31.0377	87.8606	27.772
4.24	1.0184	31.0387	88.059	27.8359
4.28	1.0384	31.0398	88.0691	27.8405

Table 7.Effect of IGZO EA on PCE

3.6 Effect of Electron Affinity of HTL on Cell Performance

The variation of the CuSbS₂ bandgap from 3.85 eV to 4.05 eV influences device performance primarily through adjustments in the HTL electron affinity, which governs interfacial energy alignment with the absorber. Since an efficient HTL must maintain its conduction band considerably higher than that of the absorber to effectively block electron back-transfer, changes in electron affinity subtly alter this offset [35]. Throughout the examined range, the V_{OC} remains essentially constant (~1.0184 V), suggesting that interfacial recombination at the HTL/absorber junction is negligible. Similarly, the J_{SC} remains stable (~31.04 mA/cm²), as light absorption and carrier generation are predominantly absorber-driven. However, the FF exhibits a minor decline from 88.07% to 87.97% with increasing bandgap, indicative of slightly less favorable carrier extraction efficiency due to subtle interfacial misalignment. Consequently, the PCE decreases marginally from 27.84% to 27.81%, emphasizing that precise tuning of HTL electron affinity is critical for sustaining optimal charge selectivity and transport.

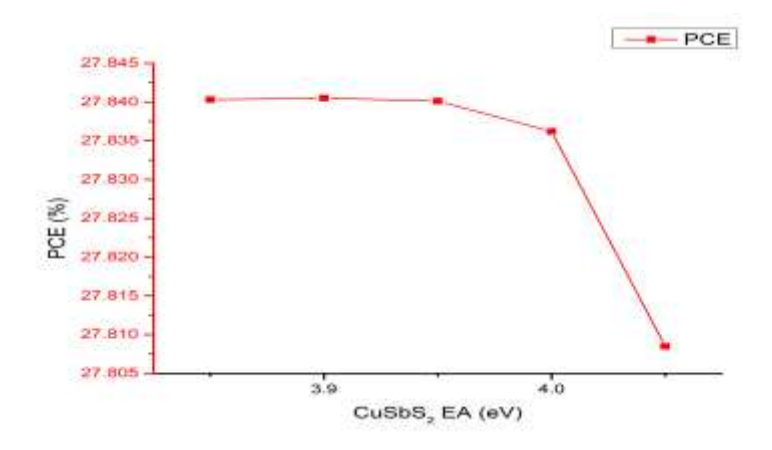


Figure 6. Effect of CuSbS₂ EA on PCE

CuSbS ₂ EA	VOC	JSC	FF	PCE
3.85	1.0184	31.0396	88.0694	27.8403
3.9	1.0184	31.0398	88.0691	27.8405
3.95	1.0184	31.04	88.0672	27.8401
4	1.0184	31.04	88.054	27.8362
4.05	1.0184	31.04	87.9657	27.8085

Table 8.Effect of CuSbS₂ EA on PCE

Structure	Thickness	PCE	Ref
FTO/TiO ₂ /RbGeI ₃ /NiO	1150 nm	10.8%	[36, 37]
ZnSe/RbGeI3/CuSCN/Au	500 nm	17.93	[38]
FTO/IGZO/RbGeI ₃ /CuSbS ₂ /Au	700 nm	29.32	This Work

Table 9 Comparison of RbGeI3 with Different ETLs and HTLs

4. Conclusion

This investigation successfully elucidated the impact of optimizing layer thickness and electron affinity within the FTO/IGZO/RbGeI₃/CuSbS₂/Au solar cell architecture on critical photovoltaic performance metrics. Systematic variation and fine-tuning of the absorber, electron transport layer, and hole transport layer parameters revealed substantial enhancements in V_{OC}, J_{SC}, FF, and PCE. The study identified that increasing the absorber thickness improved photon absorption and current generation, thereby elevating overall efficiency, with a peak PCE of approximately 29.3% at 700 nm thickness. Furthermore, optimal electron affinity values for IGZO and CuSbS₂ contributed to superior charge carrier extraction and minimized recombination losses. These findings underscore the paramount importance of meticulous

material and structural engineering in perovskite solar cells to maximize device efficacy. The intimate balance between optical absorption and charge transport layers facilitated efficient charge separation and collection, demonstrating the potential for high-performance, cost-effective photovoltaic devices. Ultimately, this work provides a robust framework for designing tailored perovskite solar cells through strategic modulation of interface energetics and layer dimensions, paving the way for further experimental validation and practical deployment in sustainable energy applications.

5. REFERENCES

1. Chabri, I., et al., SCAPS device simulation study of formamidinium Tin-Based perovskite solar Cells: Investigating the influence of absorber parameters and transport layers on device performance. Solar Energy, 2023. 262: p. 111846.

- 2. Manser, J.S., J.A. Christians, and P.V. Kamat, Intriguing optoelectronic properties of metal halide perovskites. Chemical reviews, 2016. 116(21): p. 12956-13008.
- **3.** Song, Z., et al., Photocapacitor integrating perovskite solar cell and symmetrical supercapacitor generating a conversion storage efficiency over 20%. Nano Energy, 2022. 100: p. 107501.
- **4.** Celik, I., et al., Environmental analysis of perovskites and other relevant solar cell technologies in a tandem configuration. Energy & Environmental Science, 2017. 10(9): p. 1874-1884.
- 5. Sharma, D., R. Mehra, and B. Raj, Design and comparative analysis of various planar perovskite solar cells through numerical simulation using different HTLs to improve efficiency. Optical Materials, 2022. 126: p. 112221.
- **6.** Shahbazi, M. and H. Wang, Progress in research on the stability of organometal perovskite solar cells. Solar Energy, 2016. 123: p. 74-87.
- 7. Mondal, S., A. Jain, and S. Maity, Exploring the potential of tin-based perovskite-silicon tandem solar cells through numerical analysis: A pathway to sustainable energy innovation. Solar Energy Materials and Solar Cells, 2024. 271: p. 112869.
- **8.** Khan, F., et al., Perovskite-based tandem solar cells: Device architecture, stability, and economic perspectives. Renewable and Sustainable Energy Reviews, 2022. 165: p. 112553.
- **9.** Eperon, G.E., et al., Neutral color semitransparent microstructured perovskite solar cells. ACS nano, 2014. 8(1): p. 591-598.
- **10.** Momblona, C., et al., Efficient vacuum deposited pin and nip perovskite solar cells employing doped charge transport layers. Energy & Environmental Science, 2016. 9(11): p. 3456-3463.
- **11.** Aktas, E., et al., Challenges and strategies toward long-term stability of lead-free tin-based perovskite solar cells. Communications Materials, 2022. 3(1): p. 104.
- **12.** Shao, S., et al., Enhancing the crystallinity and perfecting the orientation of formamidinium tin iodide for highly efficient Sn-based perovskite solar cells. Nano Energy, 2019. 60: p. 810-816.
- **13.** Mao, L., C.C. Stoumpos, and M.G. Kanatzidis, Two-dimensional hybrid halide perovskites: principles and promises. Journal of the American Chemical Society, 2018. 141(3): p. 1171-1190.
- **14.** Shao, Y., et al., Grain boundary dominated ion migration in polycrystalline organic—inorganic halide perovskite films. Energy & Environmental Science, 2016. 9(5): p. 1752-1759.

15. Tinedert, I.E., A. Saadoune, and M.K. Hossain, A theoretical study of all-inorganic perovskite solar cells: Computational modeling of the CsPbI3/RbGeI3 bilayer absorber structure. Journal of Physics and Chemistry of Solids, 2024. 189: p. 111951.

- **16.** Moufakkir, A., et al., Enhancing Pb-free inorganic perovskite solar cell using carbon as metal back contact and molybdenum trioxide as hole transport layer. Optik, 2024. 311: p. 171949.
- 17. Sarkar, D., et al., A comprehensive study on RbGeI3 based inorganic perovskite solar cell using green synthesized CuCrO2 as hole conductor. Journal of Photochemistry and Photobiology A: Chemistry, 2023. 439: p. 114623.
- **18.** Fan, W., et al., Design and optimization of all-inorganic lead-free perovskite solar cells with RbGeI3/KSnI3 heterojunction structure. Materials Today Communications, 2024. 40: p. 109749.
- **19.** Ekwu, M.T., et al., A Qualitative Theoretical Study of Inorganic HTM-Free RbGeI3 Based Perovskite Solar Cells Using SCAPS 1D as a Pathway Towards 3.601% Efficiency. East European Journal of Physics, 2023(1): p. 118-124.
- **20.** Loumachi, L., et al., Strengthen the Power Conversion Efficiency of Solar Cell Based RbGeI3: Numerical Approach. East European Journal of Physics, 2024(3): p. 416-424.
- **21.** Ghani, I.B.A., et al., Maximizing RbGeI3 perovskite solar cell efficiency through advanced TiO2/graphene nanocomposite electron transport layer. Optik, 2025. 320: p. 172116.
- **22.** Pindolia, G., S.M. Shinde, and P.K. Jha, Void of lead and non-carcinogenic germanium based RbGeI3 PSC using organic charge transport layers: towards a clean and green future. Journal of Materials Science: Materials in Electronics, 2023. 34(9): p. 804.
- **23.** Saikia, D., et al., Performance evaluation of an all inorganic CsGeI3 based perovskite solar cell by numerical simulation. Optical Materials, 2022. 123: p. 111839.
- 24. Sarkar, D., et al., Rbgei3 based inorganic perovskite solar cell using green synthesized Cucro2 as Htl: a comprehensive study. V. and Khan, Sobayel and Khan, MNI and Rabbani, AFM Masum and Shahinuzzaman, Md. and Aminuzzaman, Mohammod and Anuar, Farah H. and Suemasu, Takashi and sopian, Kamaruzzaman and Akhtaruzzaman, Md., Rbgei3 based inorganic perovskite solar cell using green synthesized Cucro2 as Htl: a comprehensive study, 2022.
- **25.** Huang, R. and J. Tang. Simulation studies on the electron transport layer based perovskite solar cell to achieve high photovoltaic efficiency. in Journal of Physics: Conference Series. 2021. IOP Publishing.
- **26.** Deepthi Jayan, K. and V. Sebastian, Modelling and comparative performance analysis of tin based mixed halide perovskite solar cells with IGZO and CuO as charge transport layers. International Journal of Energy Research, 2021. 45(11): p. 16618-16632.

27. Valeti, N.J., K. Prakash, and M.K. Singha, Numerical simulation and optimization of lead free CH3NH3SnI3 perovskite solar cell with CuSbS2 as HTL using SCAPS 1D. Results in Optics, 2023. 12: p. 100440.

- **28.** Madan, J., R. Pandey, and R. Sharma, Device simulation of 17.3% efficient lead-free all-perovskite tandem solar cell. Solar energy, 2020. 197: p. 212-221.
- **29.** Ali, M.S., et al., Lead-free CsSnCl3 perovskite nanocrystals: rapid synthesis, experimental characterization and DFT simulations. Physical Chemistry Chemical Physics, 2021. 23(38): p. 22184-22198.
- **30.** Abdulmalik, M.O., et al., Numerical study of 25.459% alloyed inorganic lead-free perovskite CsSnGeI3-based solar cell by device simulation. East European Journal of Physics, 2022(4): p. 125-135.
- **31.** Ait Abdelkadir, A., et al., Numerical simulation and optimization of n-Al-ZnO/n-CdS/p-CZTSe/p-NiO (HTL)/Mo solar cell system using SCAPS-1D. Results in Optics, 2022. 8: p. 100257.
- **32.** Kim, G.-W., D.V. Shinde, and T. Park, Thickness of the hole transport layer in perovskite solar cells: performance versus reproducibility. RSC advances, 2015. 5(120): p. 99356-99360.
- **33.** Gou, T., et al., Simulation and optimization of triple cation Perovskite solar cell using SCAPS-1D. Micro and Nanostructures, 2024. 189: p. 207819.
- **34.** Singh, N., A. Agarwal, and M. Agarwal, Study the effect of band offsets on the performance of lead-free double perovskite solar cell. Optical Materials, 2022. 125: p. 112112.
- **35.** Prochowicz, D., et al., Understanding the effect of chlorobenzene and isopropanol anti-solvent treatments on the recombination and interfacial charge accumulation in efficient planar perovskite solar cells. Journal of Materials Chemistry A, 2018. 6(29): p. 14307-14314.
- **36.** Pindolia, G., S.M. Shinde, and P.K. Jha, Optimization of an inorganic lead free RbGeI3 based perovskite solar cell by SCAPS-1D simulation. Solar Energy, 2022. 236: p. 802-821.
- **37.** Qin, Z., Y. Zhang, and J. Guo, SCAPS simulation and DFT study of ultra-thin lead-free perovskite solar cells based on RbGeI3. Optics Communications, 2024. 554: p. 130187.
- **38.** Talukdar, A., et al., Unveiling the role of band offset in inorganic RbGeI3-based perovskite solar cells: a numerical study in SCAPS-1D. Indian Journal of Physics, 2024. 98(12): p. 3913-3929.